Theor Chem Acc (2006) 115: 1–17
DOI 10.1007/s00214-005-0014-z

REGULAR ARTICLE

H. Gharibi · R. Behjatmanesh-Ardakani
S. M. Hashemianzadeh · S. M. Mousavi-Khoshdel
S. Javadian · B. Sohrabi

Study of thermodynamic parameters in amphiphilic systems by lattice Monte Carlo: effect of tails and heads

Received: 24 July 2004 / Accepted: 18 November 2004 / Published online: 9 November 2005

Abstract Results from three-dimensional lattice Monte Carlo simulations of amphiphile–solvent mixtures are presented. The chemical potential is derived from the monomer distribution in different clusters rather than using a Widom particle insertion approach. The effect of tail and head characteristics on the non-ideality of these systems, aggregation number, and premicellar phenomena is considered. The aggregation number and CMC behavior of the simulated amphiphilic systems are compared with existing experimental results for non-ionic amphiphiles. Two kinds of polydispersity changing with total concentration of surfactants are observed which are related to phase transition phenomena. Shape variations in clusters are studied by calculating the eigenvalues of the gyration matrix; it is shown that large clusters are non-spherical. With the Maclaurin's expansion of activity coefficient into volume fraction, the distribution of excess chemical potential with changing aggregation number is considered. Study of the degree of non-ideality of these amphiphiles reveals that asymmetric amphiphiles are characterized by greater non-ideality than symmetric amphiphiles. Goldstein's parameters are calculated taking non-ideality into consideration. The difference between the phenomenological model and the simulation data is investigated.

List of Symbols

n	Aggregation number
x_n	Mole fraction of cluster with aggregation number n
x_a	Total mole fraction of surfactant
V_s	Total volume fraction of surfactant
T	Tail part of amphiphile chain
H	Head part of amphiphile chain
h	Excess chemical potential in ideal condition
w	Water site
W	Rosenbluth weight
E	Energy of system
K_B	Boltzmann constant
ε	Interaction parameter between H–T and w–T sites
n_{Tw}	Number of tail–water interactions
n_{TH}	Number of tail–head interactions
$P_{acc.}$	Probability for acceptance of new configuration
β	Reduced temperature
$Z_s(i)$	Number of nearest water sites for site i
z	Coordination number
N_n	Number-average aggregation number
N_{wt}	Weight-average aggregation number
I_P	Polydispersity
n_{max}	Aggregation number at the maximum of monomer distribution
CMC	Critical micelle concentration
H_iT_j	An amphiphile chain with i sites in the head and j sites in the tail
C_jE_i	Non-ionic surfactant with j carbons and i ethoxylate groups
I_1, I_2, I_3	Three principal moments of inertia
$R^2_{r_i,r_j}$	Gyration matrix
$r_{i,cm}$	Position of the center of mass of a cluster in the i direction
l_1, l_2, l_3	Three characteristic lengths
μ_n	Chemical potential for cluster with aggregation number n
μ^0_n	Standard chemical potential of cluster with aggregation number n
f_n	Activity coefficient for a chain in cluster with aggregaion number n
f_1	Activity coefficient for monomer
μ^0_1	Standard chemical potential for monomer

H. Gharibi (✉) · R. Behjatmanesh-Ardakani
S. M. Mousavi-Khoshdel · S. Javadian · B. Sohrabi
Department of Chemistry, Tarbiat Modarres University,
P.O. Box 14155-4838, Tehran, Iran
E-mail: gharibi@irandoc.ac.ir

H. Gharibi
Iranian Information and Documentation Center (IRANDOC),
P.O. Box 13185-1371, Tehran, Iran

S. M. Hashemianzadeh
Department of Chemistry, College of Chemistry, Iran University
of Science and Technology, P.O. Box 16765-163, Tehran, Iran

δ	Free energy in Goldstein model
δ_b	Free energy change due to transferring the hydrocarbon parts
δ_s	Free energy change due to surface interaction
δ_e	Free energy change due to entropy of a tail move
R_c	Radius of micellar core
a	Length of lattice site
τ	Surface free energy per unit area
$P(r)$	Distribution function for end-to-end distance

1 Introduction

Surfactants are used in pure or mixed form in many industrial and biological processes [1]. The roles of surfactants within these processes are diverse because the shapes and phase behavior of surfactants vary depending on factors such as their molecular structure and concentration. This has provoked numerous theoretical, simulation, and experimental studies of surfactant behavior. Amphiphilic systems have been studied using a range of experimental techniques, including surfactant-selective electrode [2,3], SANS [4], NMR [5,6], and IR spectroscopy [4,5], and theoretical approaches such as molecular thermodynamics [7], conformational statistics [8], and the phenomenological approximation [9]. Computer simulation of amphiphilic systems is now well established. There are three principal simulation approaches: molecular dynamics, Monte Carlo, and Brownian dynamics [10]. Monte Carlo simulations vary from the simplest form, the Ising model [10], to more sophisticated lattice models [11,12], to continuous models with realistic interaction potentials [13–15].

Monte Carlo simulations of amphiphilic systems on lattices have been studied for more than 20 years. Larson [16] studied the amphiphile–oil–water phase diagram by integration of the Gibbs–Helmholtz equation. Under this approach, Larson calculated the Helmholtz free energy in the canonical ensemble with an athermal initial condition and then compared these results with zero- and first-order quasi-chemical approximation. In another work, Care [17] studied the thermodynamics of cluster formation by calculating the distribution of monomer in clusters. In lattice model self-assembly of di- and tri-block copolymers has been studied by Mattice and co-workers [18,19]. They have established scaling laws for the dependence of CMC on the interaction energy and tail length in these systems. Bernardes et al. [20] used square lattice with water–water attractions, oil–oil attractions, and water–oil repulsions to study a H_1T_2 amphiphile; they assumed that the straight conformation is more stable than the folded conformation, and then examined finite size effects, meta-stability, and relaxation time for this amphiphile. Based on the model of Bernardes et al. [20], Girardi and Figueiredo [21] calculated the degree of micellar organization, Δ, for the H_1T_3 amphiphile, which is characterized by $\Delta = P(n_{max}) - P(n_{min})$, where P is the aggregate size distribution and n_{max} and n_{min} the aggregate sizes at which P exhibits its local maximum and minimum, respectively. They additionally showed that, for a three-dimensional model, Δ goes continuously to zero as the temperature is increased.

Panagiotopoulos et al. [22] determined the phase behavior and micellization of several lattice di- and tri-block surfactants in Larson type model by histogram-reweighting grand canonical Monte Carlo simulations on a lattice model. Lisal et al. [23] studied surfactant self-assembly in a supercritical solvent using the Larson model.

In the present work we studied some thermodynamic parameters such as polydispersity, aggregation number, and premicellar concentration through lattice Monte Carlo simulation using the Rodriguez model [24]. In this model we observed phase transition for some amphiphiles and studied the effect of head and tail lengths on aggregation number and, finally, the link between head and tail lengths and non-ideality.

2 Details of the Monte Carlo simulation

2.1 Model description

In the present work we used the three-dimensional model of Rodriguez [24]. In this model, space is divided into a cubic lattice of sites that interact equally with their nearest neighbors and do not interact with other sites. This gives a lattice with a coordination number of 6. On this lattice, each water molecule occupies a single site whereas amphiphiles occupy chains of sites connected by nearest neighbor relationships. The amphiphile molecule is divided into two parts: a head part that interacts with the same potential as the water sites and a tail part that is hydrophobic. The box size is set to $50\times50\times50$ and the excluded volume and periodic boundary conditions are used to mimic bulk conditions and to allow us to fix the number of particles in the (NVT) ensemble. We included only one kind of interaction in the model, i.e. between water-like sites (H, w) and oil-like sites (T) that are not adjacent on the same chain. The total internal energy can therefore be expressed as follows:

$$\frac{E}{K_B T} = \frac{\varepsilon}{K_B T}(n_{T,w} + n_{T,H}), \tag{1}$$

where $n_{T,w}$ and $n_{T,H}$ are the numbers of tail–water and tail–head pairs, respectively, and ε is the interaction parameter. We used a value of ε=0.7, as suggested by Rodriguez [24]. For this value of the interaction parameter, observed micellization was distinguished for some of the amphiphiles tested, and a phase transition was noticed for other amphiphiles.

2.2 Metropolis Monte Carlo algorithm

This work is based on the standard Metropolis algorithm [25]. The procedure for generating initial configurations is as follows. First, a cubic lattice is considered. All of the lattice sites are occupied by water molecules through code numbers. A lattice site can be occupied by one of the three types of beads: solvent, denoted by s; head, h; or tail, t. Amphiphilic

chains, $h_i t_j$, are composed of the appropriate numbers (i, j greater than or equal to one) of h and t beads. For the distribution of amphiphilic chains, we choose a set of lattice sites randomly and then the old code numbers of these sites are replaced by the new ones. To introduce an amphiphilic chain, a lattice site is selected at random for chain growth. Growth of a chain can only be continued if at least one neighboring site is not occupied by either other chains that have been placed on the lattice or any previous unit of the trial chain that is being grown. The total energy of this initial configuration, denoted E_{old}, is then calculated according to the previous energy parameters. This initial configuration is then altered by selecting a random surfactant chain and then moving it by Monte Carlo moves, and the energy of the new, trial configuration, E_{new}, is calculated. This trial configuration is accepted according to the probability:

$$P_{\text{acc.}} = \text{Min}\{1, \exp(-\beta \Delta E)\}. \tag{2}$$

This procedure is continued until equilibrium is reached. To relax our systems we used Bernardes et al.'s approach [20]. In this method they compared the results for the average of the system for two opposite initial configurations: the first one is completely random (typical of high temperatures) and the second is completely ordered (typical of low temperature). In cases where a unique equilibrium state was attained after a finite number of trials, this test allowed evaluation of relaxation times (in MC step units). The initial relaxation configurations must be discarded when calculating equilibrium averages. Furthermore we run some of our simulations at athermal conditions and the interaction energy was increased at each step, until the desired interaction energy is reached [24]. We found that all of the three methods converge.

Once equilibrium has been reached, a large number of configurations are generated for calculating ensemble averaged thermodynamic properties. This averaging must be performed using independent configurations. The number of moves required for a system to reach a state independent of its original state has been estimated previously by calculating time correlation function [10,26] .The fluctuation of properties is reduced by taking large ensemble averages. Different initial configurations may be used to avoid metastable states.

2.3 Monte Carlo moves

Different chain moves have been reported for lattice and off-lattice simulations. Binder [27] discussed various possible moves and the microscopic reversibility conditions of them. One of the most famous chain moves is reptation. In this move one of the two ends of a chain is chosen at random, and then one of the five potentially available nearest neighbors of the selected chain end is chosen at random. If the selected site is a solvent site, the chain end is moved to that site and all of the other segments of the chain follow the end site. Whether the move is made or not, the reptation move is completed. Although the simplicity of this procedure is attractive the reptation method gives various configurations that are dependent on each other [29]. Furthermore Siepmann and Frenkel [29] show that for reptation move a large fluctuation can be observed.

For avoiding these correlations it is necessary to consider either very large configurations in constant snapshots or low snapshots in constant configurations during the simulation. The first case increases the computation time and the other case increases the fluctuation of ensemble averaging. For this reason, we apply reptation in conjunction with another move known as the configurational bias Monte Carlo move [29]. Configurational bias sampling methods are used to facilitate the insertion and removal of surfactant molecules. These methods are based on the following algorithm:

1. One chain is chosen at random for removal.
2. The Rosenbluth weight (W) for this chain is then calculated by counting the number of solvent sites ($z_s(i)$) around the next bead to be removed. For the chain that is being removed this factor is represented by W_{old}, which is defined as:

$$W_{\text{old}} = \prod_{i=m-1}^{1} \frac{z_s(i)}{z}, \tag{3}$$

   where m is the chain length.
   The product in Eq. 3 represents the total number of possible configurations of deleted chain. For deletion of the chain the end segment is deleted but is not considered in the above product because after it has been deleted we do not have any segment left to calculate its choices.
3. A lattice site is chosen at random for growing the removed chain.
4. The chain is grown. After setting each site in its place on the lattice, the possible ways that the next site can be placed are calculated. By this method the Rosenbluth weight (W) for this chain is calculated:

$$W_{\text{new}} = \prod_{i=1}^{n-1} \frac{z_s(i)}{z}. \tag{4}$$

If $z_s(i)$ becomes zero for any of the sites, then the system is returned to its old state and the configuration is not altered. Detailed balance is maintained using the ratio of the two Rosenbluth weights in the acceptance criterion:

$$P_{\text{acc.}} = \min\left\{1, \frac{W_{\text{new}}}{W_{\text{old}}} \exp(-\beta \Delta E)\right\}. \tag{5}$$

Rather than picking a solvent site at random, one can use the Boltzmann weight of sites to bias the insertion.

We used reptation and the bias move with equal probability. As shown in Fig. 1, use of bias move reduces the relaxation time.

2.4 Definition of parameters

Various properties are calculated during the simulation, including the mole fraction of monomer, mole fraction of clusters with aggregation number $n(x_n)$, monomer distribution in cluster with size $n(nx_n)$, number-average aggregation number (N_n), weight-average aggregation

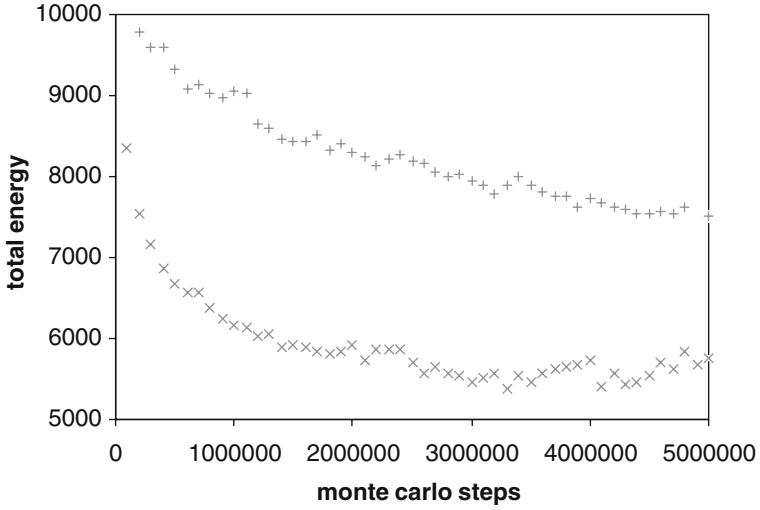

Fig. 1 Comparison of reptation (+) and (×) reptation with bias move (*blue*)

number (N_{wt}), polydispersity (I_{p}), three principal moments of inertia, and characteristic lengths. When tail sites from two different chains are nearest neighbors, the two chains are said to form an aggregate. An amphiphile that is not in an aggregate is a monomer. Three kinds of aggregation number can be defined [24]. Two of these are defined as:

$$N_n = \frac{\sum_{n=2}^{n_{\max}} n x_n}{\sum_{n=2}^{n_{\max}} x_n}, \tag{6}$$

$$N_{\mathrm{wt}} = \frac{\sum_{n=2}^{n_{\max}} n^2 x_n}{\sum_{n=2}^{n_{\max}} n x_n}, \tag{7}$$

where $n_{\max}$ is the maximum aggregation number in all configurations considered in ensemble averaging and x_n is the mole fraction of clusters with aggregation number n. The third way of defining the aggregation number is to define it based on the local maximum of the aggregate-size distribution curve in which nx_n is plotted against $n(N_{\max})$. The aggregate-size distribution curve is also referred to as the monomer distribution curve. The monomeric form is not considered an aggregate and hence is not included in the above equations. The polydispersity is defined as the ratio of N_{wt} to N_n. For clusters of size $n \geqslant 10$ in monomer distribution curve, the value of nx_n is averaged over aggregates of size $n \pm 2$ in order to reduce statistical fluctuations and to obtain a smooth distribution [24]. Aggregates comprised of less than 10 monomers are often referred to in the literature as premicelles [24].

3 Results and discussion

3.1 Critical Micelle concentration

There are different definitions for CMC in theoretical works. For example Ruckenstein and Nagarajan [30,31] have defined CMC as a point which separates two kinds of behavior of the size distribution of micellar aggregates of surfactant molecules. Below this concentration, the size distribution is a monotonic decreasing function of size; above this concentration, the size distribution is a function exhibiting two extrema and the contribution of larger aggregates becomes important. But in simulation works often two definition are used. In Care's definition [32], CMC is determined approximately by taking the intercept of a line drawn through the high concentration data with a line through the origin of unit slope. In Israelachvili's definition [33], CMC is the amphiphile concentration at which the number of aggregated amphiphiles equals the number of free amphiphiles. Rodriguez et al. [24] used Israelachvili's definition. Recently a new definition was introduced by Zaldivar and Larson [34]. They defined CMC as the intercept between a line with a slope of unity which passes through the origin and a line with zero slope that has a value equal to the average free monomer concentration after micellization. The origin of the last definition introduced by Tanford's [35] was around 25 years ago. Various definitions of CMC are introduced by different researchers but all of them have two common point of views, (a) nx_n versus n must be flat at CMC, (b) nx_n versus n should show maximum and minimum after CMC.

A feature of these definitions is that the CMC calculated using Care's definition is always less than that calculated using Israelachvili's definition. In experimental work, particularly in studies of polymer–surfactant mixtures, the CMC is often taken as the intersection between straight lines fitted to the regions before and after the maximum point in the monomer mole fraction or monomer volume fraction curve [36]. A comparison of these three definitions is shown in Fig. 2. On the basis of the three definitions, the experimentalist's definition yields CMC values that are closest to the true CMC. Comparison of the CMC values obtained using the three definitions for various systems (Table 1) reveals that the CMC values obtained using the experimentalist's definition fall between those obtained using the other definitions, except for H_4T_3. As shown in Fig. 3, the anomalous behavior of H_4T_3 is related to premicellar phenomena.

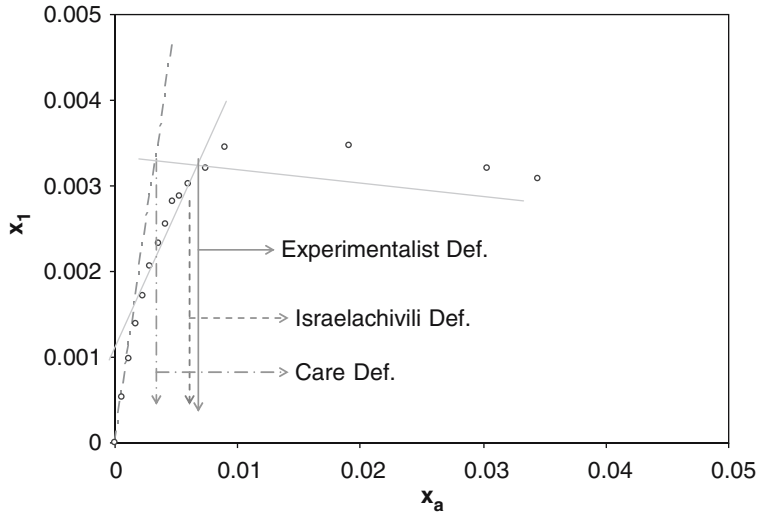

Fig. 2 Determination of the CMC of H_4T_3 using three approaches

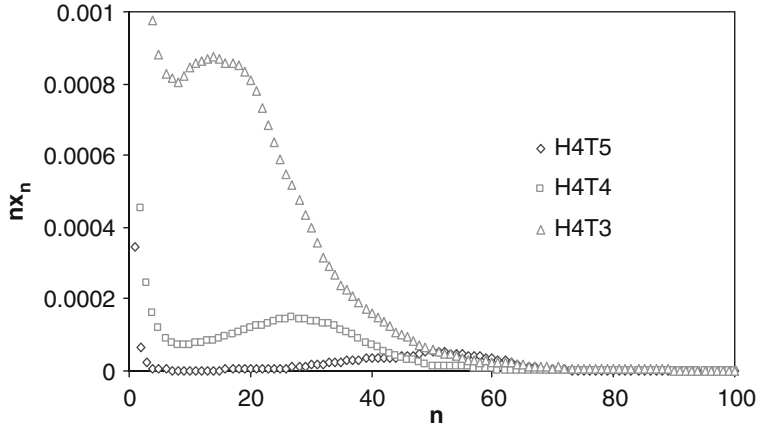

Fig. 3 Premicellar phenomena for amphiphilic systems with various tail lengths

Table 1 Comparison of CMC values obtained using three approaches

Amphiphile	Care Def.	Experimentalist Def.	Israelachvili Def.
H_1T_4	0.0007	0.0009	0.0012
H_2T_4	0.0009	0.0013	0.0017
H_3T_4	0.0012	0.0018	0.0022
H_4T_4	0.0014	0.0022	0.0025
H_4T_5	0.0004	0.0006	0.0007
H_4T_6	0.0002	0.0002	0.0003
H_4T_3	0.004	0.0064	0.006

The dependence of the CMC on tail and head length has been studied experimentally [37]. Non-ionic surfactants such as C_jE_i or other fatty alcohol alkoxylates can be represented using the notation H_iT_j by taking the alkoxy group as the head group and the alkyl group as the tail group [24]. Using this notational change from C_jE_i to H_iT_j, we analyzed the experimental data from Ref. [37] and derived the following equation for the behavior of the experimental results:

$$\log(x_{\text{cmc}}) = 0.08i - 0.47j - 3.2, \quad R^2 = 0.98, \tag{8}$$

where x_{cmc} is the total mole fraction of surfactant at the CMC and i and j the numbers of head and tail segments in each chain, respectively. In addition, by recalculating and fitting the results of Ref. [24], we derived the following equation:

$$\log(x_{\text{cmc}}) = 0.11i - 0.45j - 3.85, \quad R^2 = 0.95. \tag{9}$$

Alternatively, if the final OH and the ethyl group bonded to it in the C_jE_i structure are considered as one alkoxy group, then C_jE_i can be modeled as $H_{i+1}T_{j-2}$. Using this approach, we derived the following equation for the experimental data in Ref. [37]:

$$\log(x_{\text{cmc}}) = 0.08i - 0.45j - 4.2, \quad R^2 = 0.97. \tag{10}$$

The CMCs of non-ionic surfactants extracted from Ref. [37] and that of comparative amphiphiles in the form of H_jT_j are listed in Table 2. As is clear from the above equations, considering the final OH group as a part of the head site modifies the fitted equation.

3.2 Distribution of monomer in cluster

A plot of the proportion of monomers in clusters of size $n(nx_n)$ as a function of n typically has two maxima, one for

Table 2 Adaptation of non-ionic amphiphiles to lattice chains

Fitting of head in exp.	Fitting of head in sim.	Fitting of tail in exp.	Fitting of tail in sim.
$C_{12}E_4(H_5T_{10})$	H_1T_4	$C_{10}E_8(H_9T_8)$	H_4T_3
$C_{12}E_8(H_9T_{10})$	H_2T_4	$C_{12}E_8(H_9T_{10})$	H_4T_4
$C_{12}E_{10}(H_{11}T_{10})$	H_3Tt_4	$C_{14}E_8(H_9T_{12})$	H_4T_5
$C_{12}E_{12}(H_{13}T_{10})$	H_4Tt_4	$C_{16}E_8(H_9T_{14})$	H_4T_6
$R^2 = 0.99$	$R^2 = 0.99$	$R^2 = 0.96$	$R^2 = 0.99$

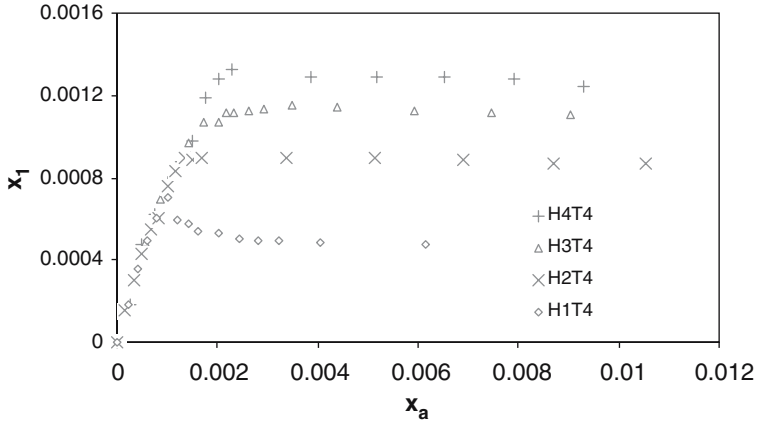

Fig. 4 Variation of monomer mole fraction for a range of amphiphiles

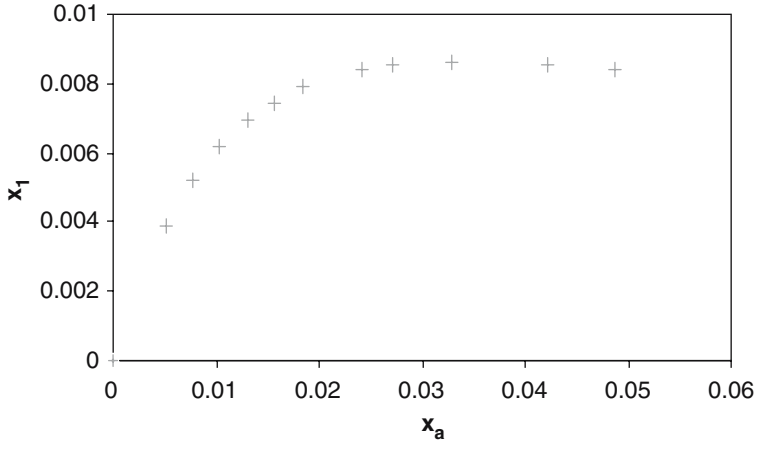

Fig. 5 Variation of monomer mole fraction for H_2T_2

the monomer and one for the micelle [38]. A wider distribution indicates a higher polydispersity. As shown in Fig. 3, the presence of high concentration of clusters with small aggregation numbers indicates the existence of premicellar phenomena. Some authors have argued that a reduction in monomer concentration is insufficient as a signature of micellar organization, and that, to unambiguously identify the onset of micellization, there should not only be a drop in monomer concentration, but also the plot of the proportion of monomers in clusters of size n as a function of aggregation number must show a local minimum and maximum [21, 17]. For this reason, we determined both the monomer mole fraction and the distribution of the amount of monomer in clusters as a function of aggregation number for all amphiphiles (Fig. 4). Among the amphiphiles we considered, only H_2T_2 did not exhibit the second maximum in the plot of the proportion of monomers in clusters as a function of aggregation number. As shown in Figs. 5 and 6, in the case of H_2T_2 the concentration of monomer decreases after a certain concentration but its distribution of monomer in clusters as a function of aggregation number does not exhibit a local minimum and maximum, indicating that H_2T_2 has not formed micelles. Inspection of a snapshot of this surfactant (Fig. 7) clearly reveals that this surfactant preferentially forms small clusters. As the number of H_2T_2 molecules in the system is increased, this amphiphile forms an increasing number of small clusters; hence the monomer concentration decreases but without the formation of micelles.

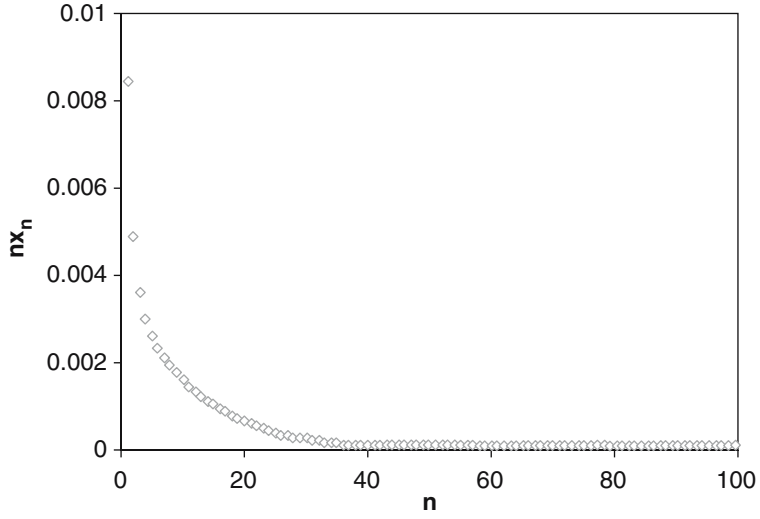

Fig. 6 Distribution of monomer in different clusters for H_2T_2

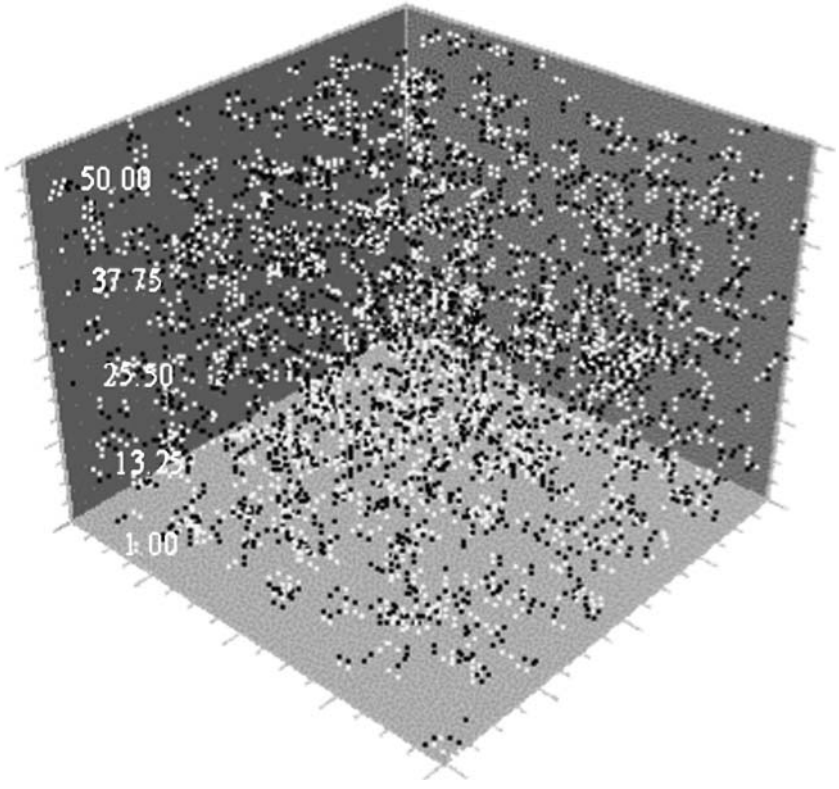

Fig. 7 Snapshot of H_2T_2 at $V_s = 0.17$ ($x_a = 0.049$)

The shape of the monomer distribution curve is also influenced by correlations between the configurations that are ensemble averaged. As shown in Fig. 8 for the H_1T_4 system, for example, simulations using bias moves to reduce correlations between configurations give a monomer distribution curve with a single maximum corresponding to micellar peak, whereas simulations using only reptation give two maxima in this curve.

Stauffer et al. [39] studied phase transitions in amphiphile systems by monitoring aggregation number as a function of CPU time. If the second maximum in the monomer distribution within clusters moves towards higher aggregation number with increasing amphiphile concentration, as is observed for H_1T_4 and H_4T_6 (Figs. 9, 10), a phase transition has occurred. In these systems, one cluster is formed and this cluster grows as further amphiphile molecules are added to

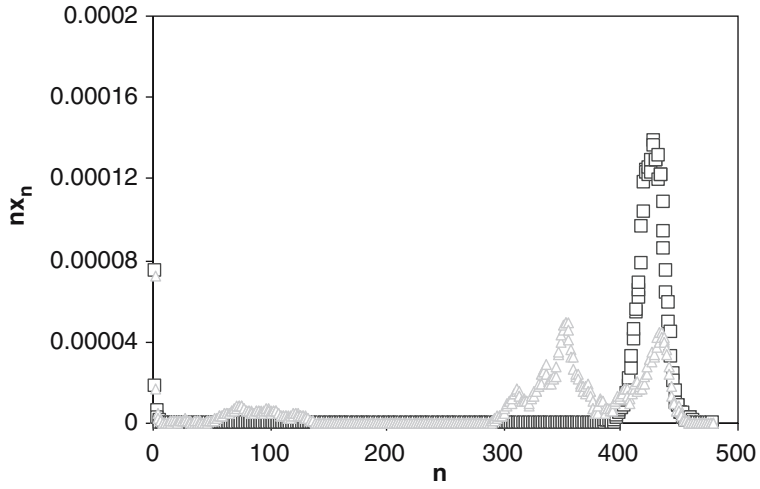

Fig. 8 *Triangles* only reptation moves and *Squares* both reptation and bias moves with equal probability

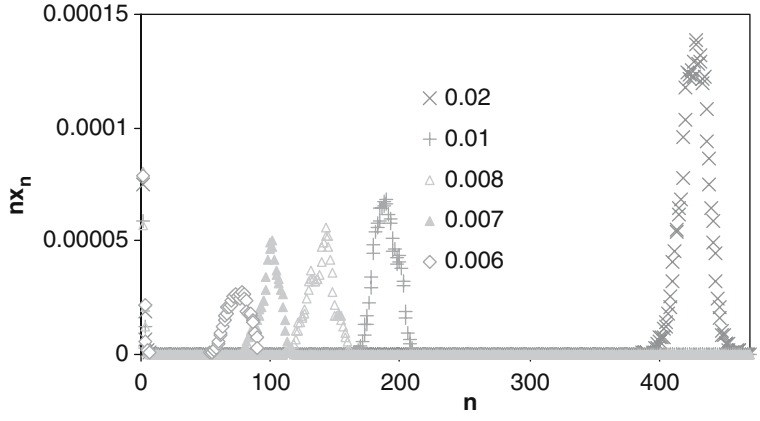

Fig. 9 Phase transition in H_1T_4

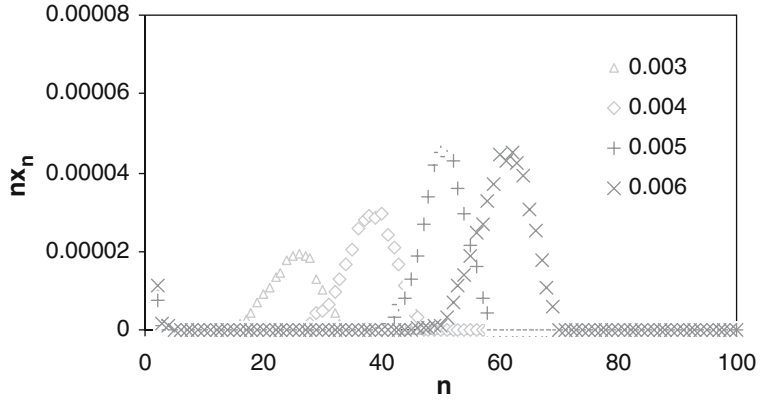

Fig. 10 Phase transition in H_4T_6

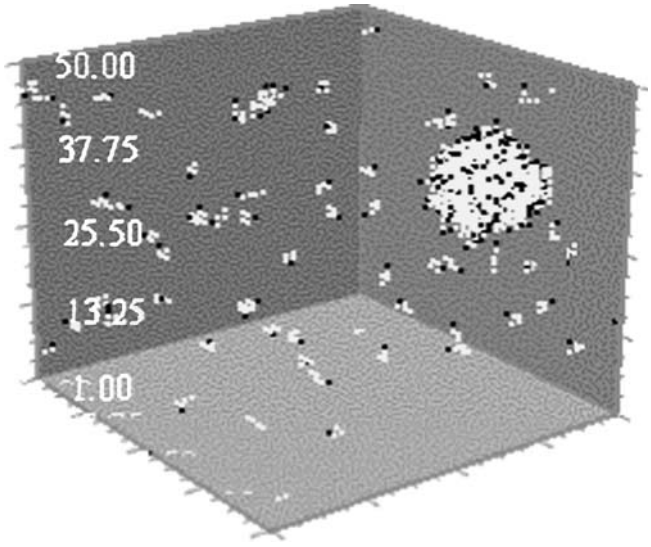

Fig. 11 Snapshot of H_1T_4 at $V_s = 0.01$ ($x_a = 0.002$). *White points* are tails

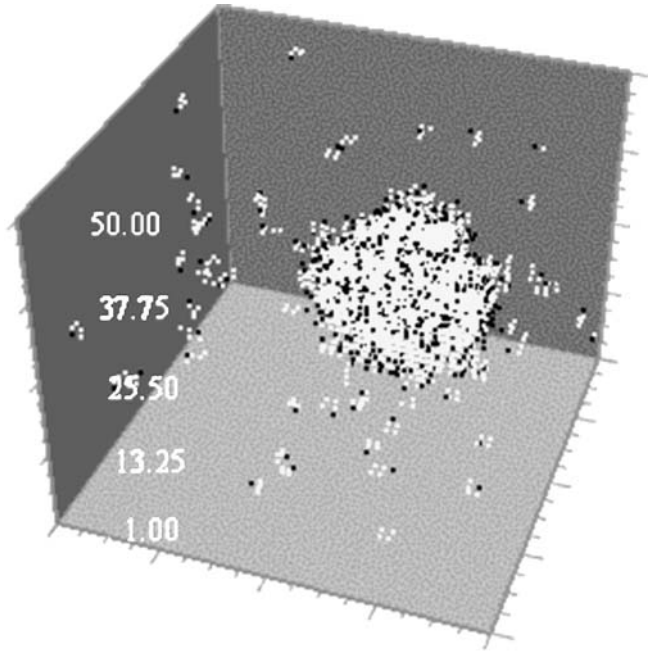

Fig. 12 Snapshot of H_1T_4 at $V_s = 0.03$ ($x_a = 0.006$)

the system, giving rise to a system with only one large cluster. This behavior is illustrated in the snapshots of the H_1T_4 system at two different concentrations shown in Figs. 11 and 12. In contrast to this tendency to form one large cluster, some amphiphiles tend to form two or more cluster shapes. One such amphiphile is H_2T_4. As shown in Fig. 13, H_2T_4 tends to form spherical clusters at lower amphiphile concentrations, but at higher concentrations it forms both spherical and non-spherical clusters (with higher aggregation number). This behavior is evident in the snapshots of systems containing 2 and 4 vol.% H_2T_4 shown in Fig. 14. In the normal case, the location of the maximum in the cluster distribution is relatively insensitive to the amphiphile concentration, as is shown for H_3T_4 in Fig. 15.

3.3 Polydispersity

Polydispersity is the ratio of the weight-average aggregation number to the number-average aggregation number. The CMC may be defined as the amphiphile concentration at which the rate of change of the polydispersity with changing concentration is greatest. In normal cases, it is expected that as the surfactant concentration is increased beyond the CMC, the polydispersity should decrease because the addition of further surfactant molecules will lead to the growth of smaller clusters and thus the distribution of cluster aggregation numbers will be narrowed. This behavior is indeed observed for H_4T_5, as shown in Fig. 16. For H_1T_4, which undergoes a phase transition with increasing concentration, the polydispersity is expected to remain approximately constant after the CMC; this behavior is observed as shown in Fig. 17. The tendency to grow one cluster (H_1T_4 or H_4T_6) or to form some large clusters (H_2T_4), leads to a wider distribution of cluster aggregation numbers.

3.4 Micellar shape

To determine the micellar shapes, we use the three principal moments of inertia, I_1, I_2, I_3. These moments are the eigenvalues of the matrix of the radii of gyration, which are defined as:

$$R^2_{r_i,r_j} = \frac{1}{S}\sum_{k=1}^{s}(r_{i,k} - r_{i,\mathrm{cm}})(r_{j,k} - r_{j,\mathrm{cm}}), \tag{11}$$

where r_i, $1 \leqslant i \leqslant 3$, represents lattice direction and $r_{i,\mathrm{cm}}$ is the center of mass in direction i, which is given by:

$$r_{i,\mathrm{cm}} = \frac{1}{S}\sum_{k=1}^{S} r_{i,k}. \tag{12}$$

Here S is the total number of sites occupied by the aggregated form. The characteristic lengths are defined as $l_i = (I_i)^{1/2}$.

3.4.1 Spherical shape

For spherical aggregates, $l_1/l_3 = l_2/l_3 = 1$, as shown in Fig. 18. Some amphiphiles always form spherical aggregates, even at high concentration. One such amphiphile is H_4T_4. Some other amphiphiles, for example H_2T_4, form spherical aggregates at low concentration (Fig. 19) but rod-like aggregates at higher concentrations.

3.4.2 Cylindrical shape

For cylindrical micelles, $l_1/l_3 \gg 1$ and $l_2/l_3 = 1$. Figures 18 and 20 show the variation in the characteristic length for H_2T_4 at concentrations of 1 and 4 vol. %. The aggregate shape was

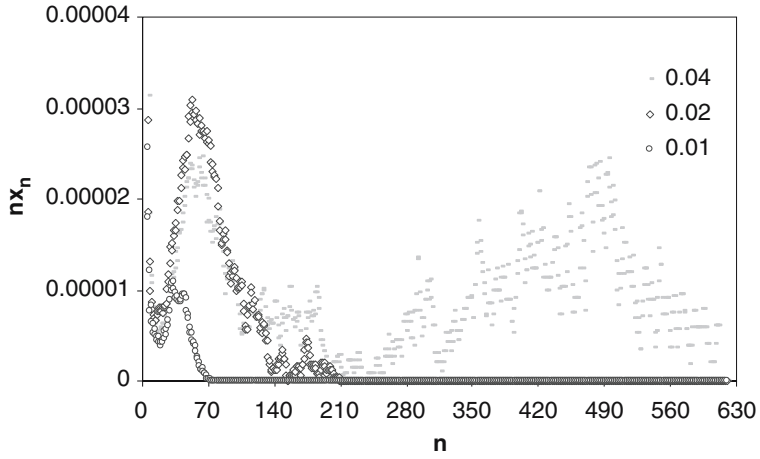

Fig. 13 Two aggregate shapes of H_2T_4 are formed at nearly $V_s = 0.04$

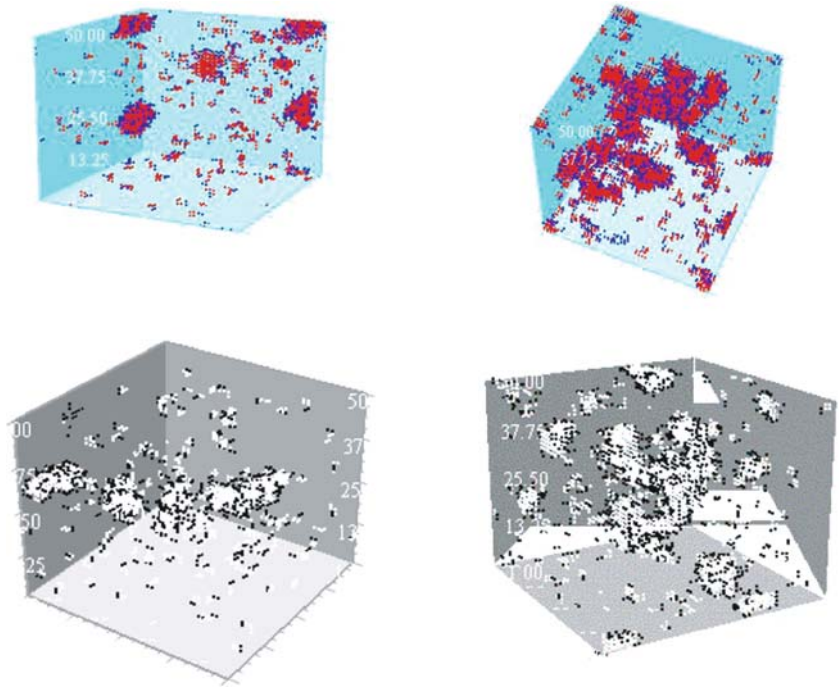

Fig. 14 H_2T_4 at $V_s = 0.02$ ($x_a = 0.003$) (*left*) and $V_s = 0.04$ ($x_a = 0.007$) (*right*)

also gleaned by directly visualizing the lattice configurations generated from the simulation at various concentrations. As shown in Figs. 19 and 21, the shapes of the aggregates change from spherical to rod-like with increasing concentration.

3.5 Aggregation number: effect of tail and head

Previous experimental studies on C_jE_i non-ionic amphiphiles have additionally examined the relationship between aggregation number and tail and head lengths [37]. Modeling C_iE_j as $H_{j+1}T_{i-2}$, we compared the previous experimental data with our simulation results. We chose to make this comparison for systems whose concentration was twice the CMC. The following equations were derived from the simulation data:

$$N_{\max} = 1.8\exp(0.6j), \quad R^2 = 0.96 \quad \text{for} \quad \text{tail},$$
$$N_{\max} = 294\exp(-0.7i), \quad R^2 = 0.95 \quad \text{for} \quad \text{head}, \qquad (13)$$

where $N_{\max}$ is the aggregation number corresponding to the local maximum in the monomer distribution at a concentration of twice the CMC, and i and j are the number of head and tail segments in the amphiphile, respectively. For the adapted experimental data, the fitted equations are:

$$N_{\max} = 0.14\exp(0.7j), \quad R^2 = 0.95 \quad \text{for} \quad \text{tail},$$
$$N_{\max} = 2,600\exp(-0.2i), \quad R^2 = 0.7 \text{ for} \quad \text{head}. \qquad (14)$$

As in the case of the CMC, the tail result for the aggregation number is more consistent with the experimental data than

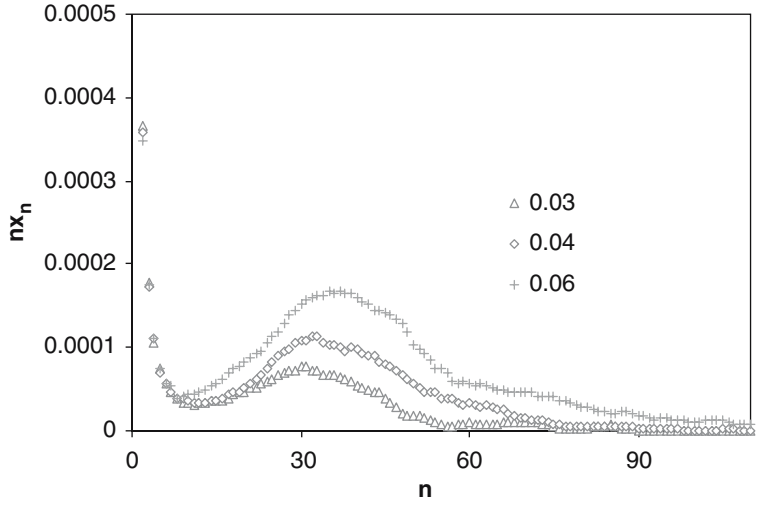

Fig. 15 Cluster distributions for H_3T_4 at various volume fractions

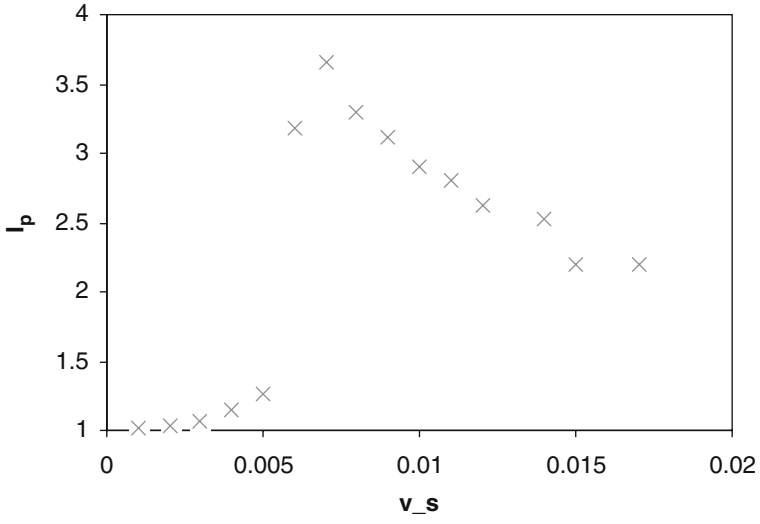

Fig. 16 Reduction of polydispersity with increasing amphiphile concentration for H_4T_5 (above CMC)

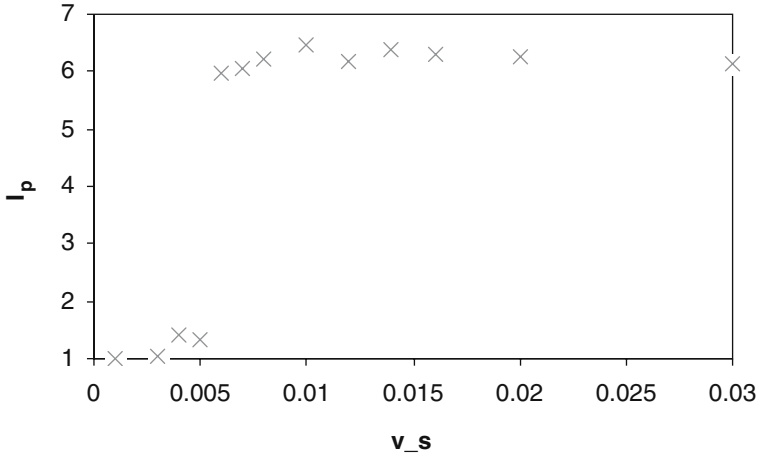

Fig. 17 Polydispersity as a function of concentration for H_1T_4

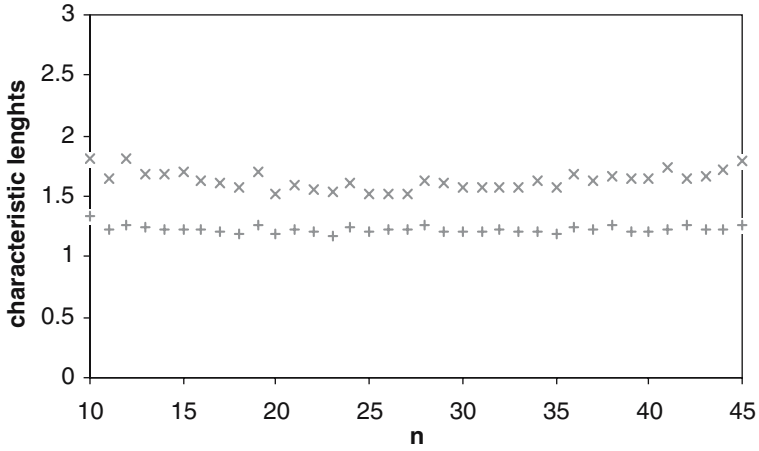

Fig. 18 Formation of spherical micelles at 1 vol.% of H_2T_4

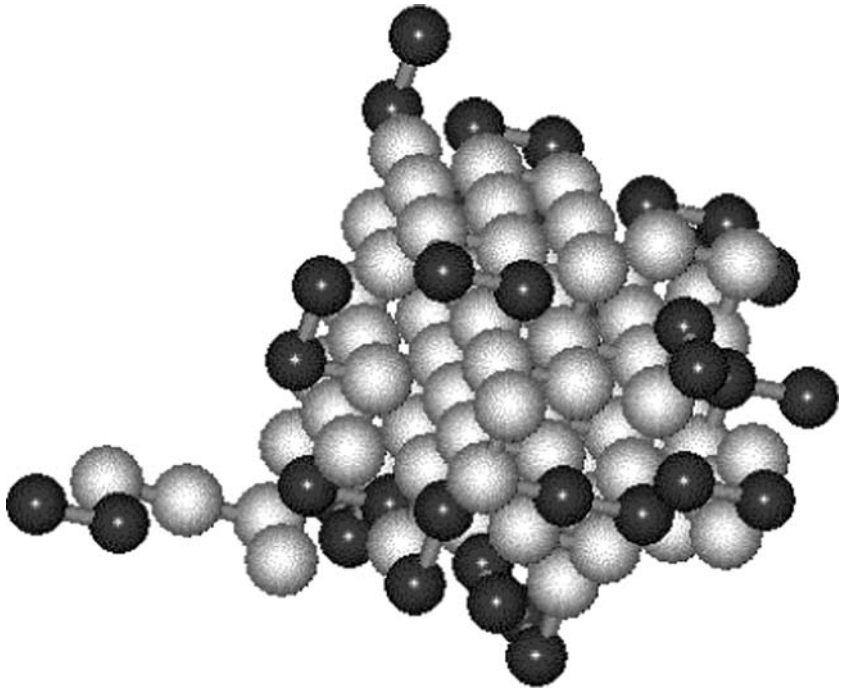

Fig. 19 Micelle of H_2T_4 at $V_s = 0.01$ ($x_a = 0.002$), *gray beads* are tails

the head result. The discrepancy between the simulation and experimental results can be attributed to the assumption of zero interaction between heads in the simulation. Although we can qualitatively compare the adapted experimental data with simulation data, quantitative evaluation is not easy. The most important issue complicating any quantitative comparison is the definition of temperature in the experiments and simulations. The lack of a consistent definition means that we cannot easily correlate temperature in the lattice simulations with that measured experimentally. An additional problem concerns the interaction parameters. In the simulations we consider that H–T and S–T interactions are of equal strength and that the H–H interaction is zero; however, these assumptions may not be true for real amphiphiles. In some amphiphiles, the H–H interaction is attractive whereas in others it is repulsive. In addition to the above concerns, in the present work we did not consider the effects of chain stiffness and other factors such as cluster formation of water molecules, non-equality of equilibration distances (parameter σ) of water molecules and amphiphile molecules, hydrogen bonding between some kinds of amphiphiles and water molecules and triplet interactions. Variation of these factors will affect the results.

3.6 Non-ideality effect

The CMC and monomer distribution in clusters can be determined from the condition that at thermodynamic equilibrium the free energy of the amphiphile system must be a minimum.

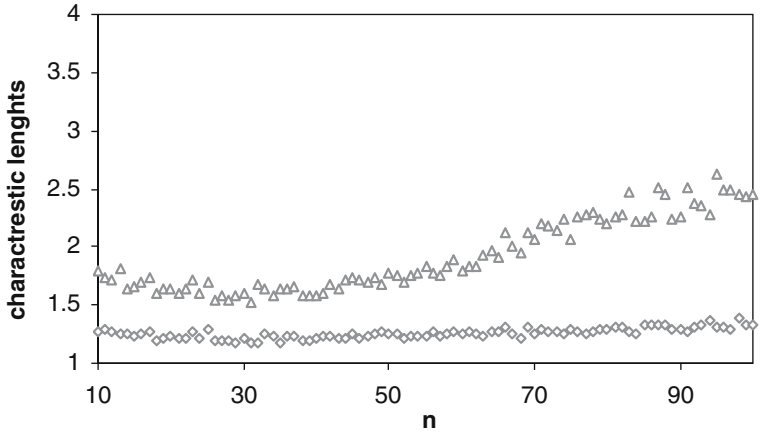

Fig. 20 Characteristic lengths of H_2T_4 at $V_s = 0.04$ ($x_a = 0.007$)

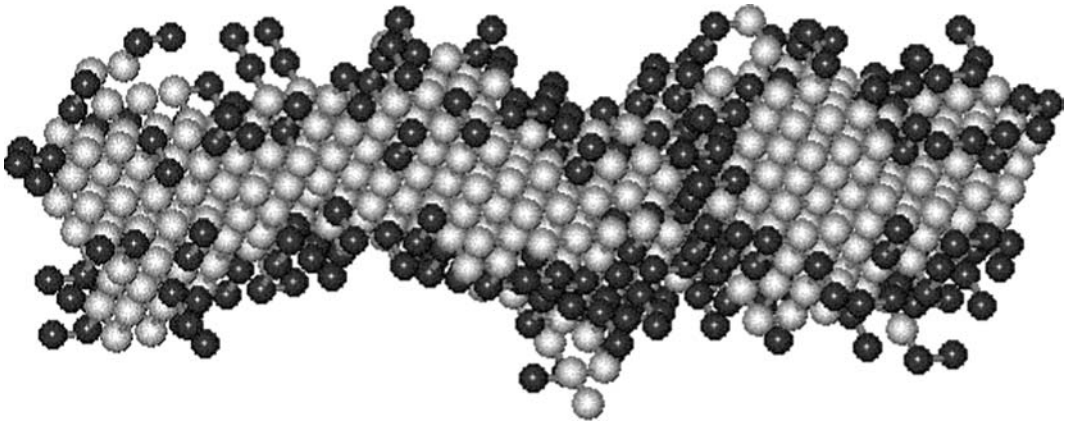

Fig. 21 Micelle of H_2T_4 $V_s = 0.04$ ($x_a = 0.007$)

The chemical potential of aggregates with n molecules can be expressed as:

$$\mu_n = \mu_n^0 + K_B T \ln(f_n x_n), \tag{15}$$

where μ_n^0 is the standard chemical potential for a cluster with aggregation number n, f_n the activity coefficient of an aggregate containing n amphiphiles and x_n the mole fraction of a cluster with aggregation number n in solution. The equilibrium micelle size distribution is that which minimizes the free energy; it is fulfilled by the relation [11,40]:

$$n\mu_1 = \mu_n. \tag{16}$$

Using Eq. 15 for μ_n, we obtain:

$$x_n = \frac{(f_1 x_1)^n}{f_n} \exp\left(-n\beta\left(\frac{\mu_n^0}{n} - \mu_1^0\right)\right). \tag{17}$$

This equation is derived by considering the multiple equilibrium model in amphiphile systems. $\left((\mu_n^0/n) - \mu_1^0\right)$ is the difference in standard Gibbs free energy between an amphiphilic molecule in an aggregate of size n and a free amphiphile in the solvent [24] and can be referred to as the excess chemical potential of chains belonging to a cluster of size n [32]. In general there is no simple way to determine the activity coefficients of the aggregates, which contain information on the inter-aggregate interactions. Desplat and Care [32] conjectured that the activity coefficients may be functions of the amphiphile concentration with the property that

$$\lim_{x_a \to 0} f_1(x_a) = \lim_{x_a \to 0} f_n(x_a) = 1 \quad \forall n$$
$$\Rightarrow \lim_{x_a \to 0} \ln f_1(x_a) = \lim_{x_a \to 0} \ln f_n(x_a) = 0. \tag{18}$$

It can be considered a Maclaurin's expansion [41] of $\ln f_n$ as a function of total mole fraction or total volume fraction [32]:

$$\ln f_n = \ln f_n(x_a = 0) + \left|\frac{\partial \ln f_n}{\partial x_a}\right|_{x_a=0} (x_a) + \frac{1}{2}\left|\frac{\partial^2 \ln f_n}{\partial x_a^2}\right|_{x_a=0} (x_a)^2 + \cdots. \tag{19}$$

By Eq. 18, the first term is equal to zero; hence

$$\ln f_n = \left|\frac{\partial \ln f_n}{\partial x_a}\right|_{x_a=0} (x_a) + \frac{1}{2}\left|\frac{\partial^2 \ln f_n}{\partial x_a^2}\right|_{x_a=0} (x_a)^2 + \cdots. \tag{20}$$

Replacing the derivative terms with parameters, we obtain:

$$\ln f_n = a_n x_a + b_n x_a^2 + \cdots. \tag{21}$$

Expressing Eq. 17 in the logarithmic form gives

$$\ln(x_n) = n\ln(x_1) + n\ln(f_1) - \ln(f_n) - n\beta\left(\frac{\mu_n^0}{n} - \mu_1^0\right) \tag{22}$$

and with substitution of Eq. 21 into 22 we obtain

$$\ln(x_1) - \frac{1}{n}\ln(x_n) = \beta\left(\frac{\mu_n^0}{n} - \mu_1^0\right) + (-a_1 + \tfrac{a_n}{n})x_a + (-b_1 + \tfrac{b_n}{n})x_a^2 + \cdots . \tag{23}$$

The left-hand side of Eq. 23 can be shown by the h function:

$$h = \ln(x_1) - \frac{1}{n}\ln(x_n), \tag{24}$$

$$-nh = -\ln(x_1)^n + \ln(x_n) = \ln\left(\frac{x_n}{x_1^n}\right). \tag{25}$$

From Eq. 25 we can say that h represents the excess chemical potential for an ideal system (i.e., a system without any interactions). For the ideal system, h is independent of the mole fraction of amphiphile.

Since x_1 and x_n are measured within the simulations for different x_a, we can plot h as a function of x_a. Then, based on Eq. 23, we can derive the excess chemical potential by determining the intercept in the plot of h versus x_a. In an ideal system the activity coefficient equals one and hence the slope must be zero. Thus the magnitude of the slope of the plot of h as a function of x_a provides a measure of the degree of non-ideality of these systems. Here we quantify the extent of non-ideality by measuring the difference of this slope from zero.

The function h for H_4T_4 is plotted in Fig. 22. The variations in the slope (non-ideality) and intercept (excess chemical potential) as a function of aggregation number are shown in Figs. 23 and 24.

3.7 Effect of head and tail on non-ideality

Because the CMC changes with increasing number of head or tail segments, in the non-ideality calculations we considered all systems at twice their respective CMCs. For the h function to be calculatable, true micellization must have occurred in the system. If a system undergoes a phase transition with increasing amphiphile concentration, such as in the H_1T_4 and H_4T_6 systems, we cannot determine the h function because, for a range of aggregation numbers, the concentration of clusters at each aggregation number does not change continuously with increasing amphiphile concentration. In these systems, most of the clusters with aggregation numbers between 1 and N_{max} have concentrations of zero, yet we need to determine the h function at different amphiphile concentrations that have the same range of aggregation number. In systems that undergo true micellization, all clusters with aggregation numbers between monomer and N_{max} are included in the ensemble average.

For the reasons outlined above, we calculated the slope of the h function at twice the CMC for all systems except H_1T_4 and H_4T_6. The slopes of the h function, which provide a measure of non-ideality, with Maclaurin's expansion of $\ln f_n$ as a function of total volume fraction for the various surfactants are listed in Table 3. The symmetric amphiphile H_4T_4 exhibited the lowest degree of non-ideality. Increasing or decreasing the number of tail segments increases the non-ideality, and the effect of changes in the number of tail segments is stronger than that of head segments. As shown in Table 3, increasing the number of head segments causes a reduction in the slope. In these amphiphiles, the greatest enhancement of non-ideality comes from increasing the number of tail segments.

Table 3 Deviation of slope of h function from zero in selected amphiphiles

Surfactant	Slope
H_2T_4	−5.89
H_3T_4	−3.16
H_4T_4	−2.16
H_4T_5	−5.86
H_5T_4	−3.12
H_4T_3	−2.26

Goldstein [11] has proposed a model for phase equilibrium in micellar solutions of non-ionic surfactants. In his model, excess chemical potential is the sum of three terms that can be labeled as bulk, surface, and entropic terms:

$$\mu_n^0 - n\mu_1^0 = n\delta = n(\delta_b + \delta_s + \delta_e). \tag{26}$$

In this equation, δ_b is the free energy change due to transferring the hydrocarbon parts from the aqueous environment to the micellar core. In Goldstein's model this term is proportional to the chain size. δ_s is proportional to the core surface area $4\pi R_c^2$. If the micelles are spherical, we can write $(4\pi/3)R_c^3 = jna^3$, where j is the number of tail segments in the amphiphile chain, n the aggregation number, and a^3 the volume of lattice site; hence [11]:

$$n\delta_s = \tau[4\pi R_c^2] = \gamma[n(i+j)]^{2/3}, \tag{27}$$

where $\gamma = (9\pi)^{1/3}\tau a^2$ and τ is the surface free energy per unit area. For the entropic term, Goldstein assumed that surfactants can be described as ideal random walk chains and compared the entropy of a free chain with that of a chain whose mean extension is equal to the core radius. The probability distribution function for end-to-end distance of a random walking chain is Gaussian [11]:

$$P(r) = \text{const.}\exp(-3r^2/2ja^2), \tag{28}$$

where $j^{1/2}a$ is the average extension of an ideal chain of fully extended length ja. The entropy as a function of the chain extension is $S(r) = K_B\ln(P(r))$; hence the entropy contribution to the free energy change is [11]:

$$n\delta_e = -nK_BT\{\ln[P(R_c)] - \ln[P(j^{1/2}a)]\} = nK_BT[c(i+j)^{-1/3}n^{2/3} - 3/2], \tag{29}$$

where c is a pure geometrical factor and is of order unity.

Hence the total free energy change is [11]:

$$\delta/K_BT = -(i+j+1.5) + \gamma(i+j)^{2/3}n^{-1/3} + (i+j)^{-1/3}n^{2/3}. \tag{30}$$

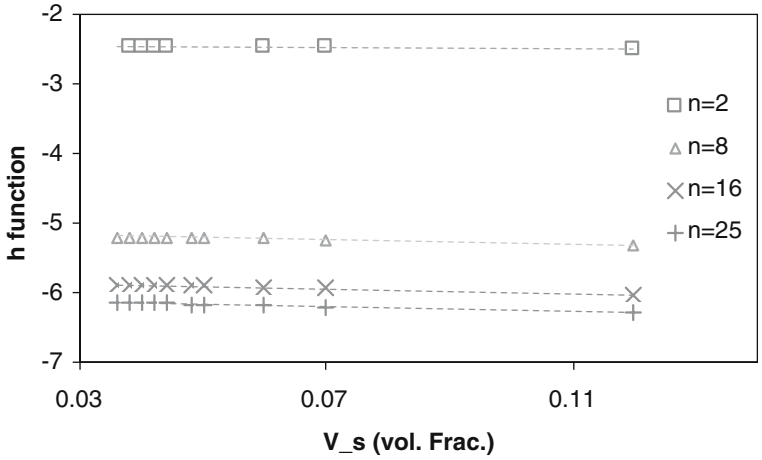

Fig. 22 Variations of h function with volume fraction of H_4T_4 for four aggregation numbers

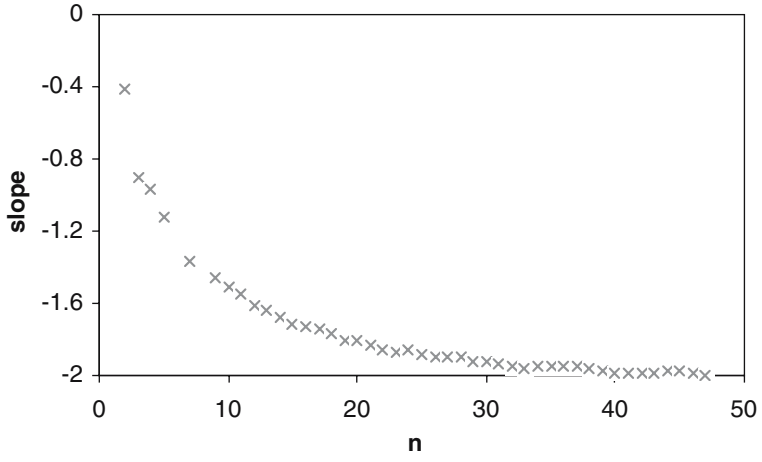

Fig. 23 Variation of slope of h function with aggregation number for H_4T_4

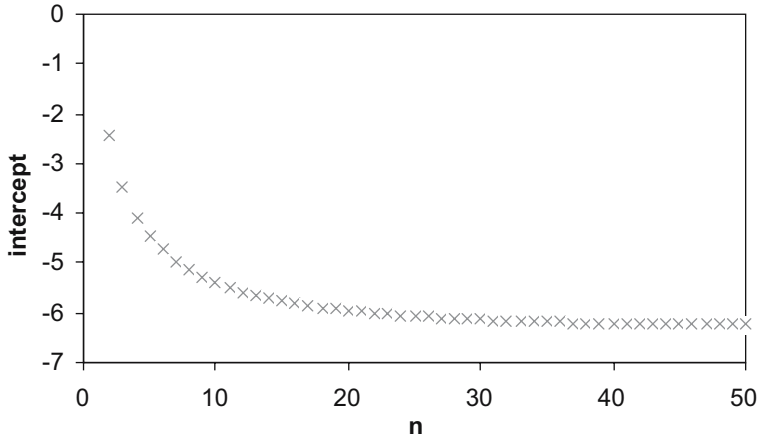

Fig. 24 Variation of excess chemical potential with n for H_4T_4

We investigated the effect of tail length on the excess chemical potential, obtained from the intercept of the h function. If these effects are fitted, the following equation is derived:

$$\delta/K_{\mathrm{B}}T = -(2.17j + 1.22) + 2.8j^{0.86}n^{-1/3} + 1.5j^{-1.77}n^{2/3}. \quad (31)$$

Because we neglected the H–H interaction, we could not determine a correct expression for the head effect. The first term in Eq. 31 is derived from the transfer of the tail to the micellar core. However, because we assume that the head–head interaction is negligible, the micelle is stabilized in the simulation to a greater extent than would be the case in the real system. Thus the first term in Eq. 31 derived from simulation data will have too strong an effect. The difference in the values of second term for simulation and phenomenological model is attributed to the shapes of the micelles. Because we used surfactants with a range of shapes, the average shape will not be that of the symmetrical amphiphile. The third term comes from the entropic contribution. The difference in the values of the third term for simulation and phenomenological model is greater than in the first two terms because Goldstein used an approximation that is not correct for short hydrocarbons; specifically, ideal random walk statistics are not valid for short chains. Besides these reasons, we have shown here that amphiphile systems are not ideal even at low concentrations due to interactions between aggregated forms that are neglected in theoretical treatments of these systems.

4 Concluding remarks

We have studied various phenomena, including phase transition behavior, micellization, and non-ideality, in a simple lattice model of an amphiphile–solvent mixture. The effect of the length of the heads and tails of the amphiphiles on the CMC, aggregation number distribution, non-ideality, and concentration of premicelles was investigated and, for selected systems, the results were compared with experimental results for $\mathrm{C}_j\mathrm{E}_i$. The simulation results were found to correspond more closely with the experimental data for tail effects compared to head effects. The discrepancy observed between the experimental and simulation results for the head effects can be attributed to the assumption in the simulations that head–head interactions in these systems are negligible. Overall, the simulation results were qualitatively consistent with the experimental results. Two types of phase transition were observed, one for $\mathrm{H}_1\mathrm{T}_4$ and the other for $\mathrm{H}_2\mathrm{T}_4$. For $\mathrm{H}_1\mathrm{T}_4$, a single cluster formed and this cluster grew as the amphiphile concentration increased. For $\mathrm{H}_2\mathrm{T}_4$, in contrast, a third peak appeared in the monomer distribution at high monomer concentration, indicating that phase transition occurred. Study of the polydispersity behavior of these systems revealed that, as the amphiphile concentration is increased, the polydispersity tends to remain constant for systems that undergo a phase transition but tends to decrease for systems undergoing micellization. It was additionally found that increasing the number of tail sites has a greater effect on the non-ideality of these systems than increasing the number of head sites. Comparison of our simulation results with the phenomenological model of Goldstein for excess chemical potential revealed that in spite of the results of Desplat and Care [32] head–head interaction affects the stabilization of micelles. It is shown that the assumption used by Goldstein in the entropy calculation, as well as his assumption that these amphiphilic systems can be treated as ideal, is incorrect.

References

1. Degiorigo V, Corti M (eds) (1985) Physics of amphiphiles: micelles, vesicles and microemulsions. North-Holland, Amsterdam
2. Gharibi H, Razavizadeh BM, Hashemianzadeh M (2000) Colloids Surf A Physicochem Eng Aspects 174:375
3. Gharibi H, Javadian S, Hashemianzadeh M (2004) Colloids Surf A Physicochem Eng Aspects 232:77
4. Penfold J, Staples E, Cummins PG (1992) Physica B 180A:537
5. Mikhalikin AP (1994) Colloid J 56:336
6. Razavizadeh BM, Mousavi-Khoshdel M, Gharibi H, Behjatmanesh-Ardakani R, Javadian S, Sohrabi B (2004) J Colloid Interface Sci 276:197
7. Shimizu K, Iwatsuru M (1990) Chem Pharm Bull 38:1353
8. Szlifer I, Ben-Shaul A, Gelbart WM (1985) J Chem Phys 83:3597
9. Nagarajan R, Ruckenstein E (1983) J Colloid Interface Sci 91:500
10. von Gottberg FK, Smith KA, Hatton TA (1997) J Chem Phys 106:9850
11. Goldstein RE (1986) J Chem Phys 84:3367
12. Widom B (1984) J Phys Chem 88:6508
13. Gunn JR, Dawson KA (1992) J Chem Phys 96:3152
14. Hansen A, Schick M, Stauffer D (1991) Phys Rev A 44:3686
15. Karaborni S, O'Connell JP (1990) J Phys Chem 94:2624
16. Larson RG (1988) J Chem Phys 89:1642
17. Care CM (1987) J Chem Soc Faraday Trans 83:2905
18. Wang Y, Mattice WL, Napper DH (1993) Langmuir 9:66
19. Wang Y, Mattice WL, Napper DH (1992) Macromolecules 25:4073
20. Bernardes AT, Henriques VB, Bisch PM (1994) J Chem Phys 101:645
21. Girardi M, Figueiredo W (2000) J Chem Phys 112:4833
22. Panagiotopoulos AZ, Floriano MA, Kumar SK (2002) Langmuir 18:2940
23. Lisal M, Hall CK, Gubbins KE, Panagiotopoulos AZ (2002) J Chem Phys 116:1171
24. Rodriguez-Guadarrama LA, Talsania SK, Mohanty KK, Rajagopalan R (1999) Langmuir 15:437
25. Metropolis N, Rosenbluth AW, Rosenbluth MN, Teller AH, Teller E (1953) J Chem Phys 21:1087
26. Nelson PH (1998) PhD Thesis simulation of self-assembled polymer and surfactant systems, Massachusetts Institute of Technology
27. Binder K (ed) (1995) Monte Carlo and molecular dynamics simulations in polymer science. Oxford University Press, New York
28. De Gennes PG (1979) Scaling concepts in polymer physics. Cornell University Press, Ithaca
29. Siepmann JI, Frenkel D (1992) Mol Phys 75:59
30. Ruckenstein E, Nagarajan R (1975) J Phys Chem 79:2622
31. Ruckenstein E, Nagarajan R (1981) J Phys Chem 85:3010
32. Desplat J-C, Care CM (1996) Mol Phys 87:441
33. Israelachvili JN, Mitchell DJ, Ninham BW (1976) J Chem Soc Faraday Trans 2 72:1525
34. Zaldivar M, Larson RG (2003) Langmuir 19:10434
35. Tanford C (1991) The hydrophobic effect: formation of micelle and biological membrane. Krieger, Malabar
36. Gharibi H, Rafati AA, Feizollahi A, Razavizadeh BM, Safarpour MA (1998) Colloid Surf A Physicochem Eng Aspects 145:47
37. Rosen MJ (1989) Surfactants and interfacial phenomena, 2nd edn. Wiley, New York

38. Aniansson EAG (1978) Ber Bunsenges Phys Chem 82:981
39. Stauffer D, Jan N, He Y, Pandly RB, Marangoni DG, Smith-Palmer E (1994) J Chem Phys 100:6934
40. Wennerström H, Lindmann B (1979) Phys Rep 52:1
41. Arfken GB, Weber HJ (2001) Mathematical methods for physicists, 5th edn. Academic, New York